Advanced Ceramics Progress: Vol. 7, No. 1, (Winter 2021) 11-17

Advanced Ceramics Progress

Research Article

Journal Homepage: www.acerp.ir

Synthesis and Characterization of Palladium Impregnated MIL-53(Fe) as Cathode Material of Supercapacitor

B. Chameh [a], M. Moradi [a] *, S. Hajati [a], F. Alikhani Hessari [a], M. A. Kiani [b]

[a] *Department of Semiconductors, Materials and Energy Research Center (MERC), Meshkindasht, Alborz, Iran*

[b] *Chemistry & Chemical Engineering Research Center of Iran, Tehran, Tehran, Iran*

ARTICLE INFO

Article History:

Received 26 September 2020
Received in revised form 19 October 2020
Accepted 29 October 2020

Keywords:

Decoration
Metal Organic Framework
Capacitance
Electrochemistry
Nanoparticle

ABSTRACT

Recently, Metal Organic Frameworks (MOFs) have been widely applied due to their high energy storage capacitance, customizable pore sizes, and open metal sites; however, their application in the form of electrode materials has been restricted due to their poor electrical conductivity. The present study reports the fast synthesis of MIL-53(Fe) and Pd/MIL-53(Fe) using the solvothermal method. To assess the electrochemical potential of materials and better understand the role of palladium in the presence of MOF, the electrodes of materials were constructed and electrochemical performances of both samples were investigated based on cyclic voltammetry in 6 M KOH electrolyte. Due to the existence of Pd in redox reaction and larger surface area, the Pd/MIL-53(Fe) showed greater electrochemical efficiency and higher specific capacitance than MIL-53(Fe). The obtained results also indicated that designing MOF via decoration of noble metal nanoparticle (MOF/noble metal) would find potential applications in the field of supercapacitors and catalysis.

https://doi.org/10.30501/acp.2020.250166.1045

1. INTRODUCTION

Over the past two decades, owing to their unique characteristics, Metal Organic Frameworks (MOFs) have drawn a great deal of attention in a variety of applications [1]. They have been widely used due to their capability to take in chemical and structural modifications through different metals, bridging ligands, and synthesis methods [2,3] and to offer considerable flexibility for tuning topologies, sizes, and pore structures [4–6]. These characteristics ensure their promising candidacy for applications such as gas storage and separations [8], catalyst [9], drug delivery and imaging [10], and conversion and energy storage devices such as fuel cells, batteries, and supercapacitors [11]. However, shuffled orientations are regarded as the main obstacle for these compounds [12]. They have relatively low electrical conductivity owing to the insulating characteristic of the organic linkers and poor overlap between π and d orbitals of the metal ions [13], limiting the effective application of built-in redox centers, hence low power density and capacitance [14,15].

Noble metal-based materials are regarded as ideal additives of electrode materials due to their enhanced chemical and thermal stability of the electrode materials. Moreover, they make feasible the movement of electrons from the electrode/electrolyte interface to the current collectors. Noble metal particles increase the capacitance of the electrical double layer by supplying wider electrochemically active surface areas for adsorption of ions. These metals commonly include a group of platinum (palladium, ruthenium, platinum, iridium, rhodium, osmium), gold, and silver [16]. However, their combination with other sustainable and cheap materials is considered one of the most desirable ways of maximizing material properties and usage due to their

* Corresponding Author Email: 2m.alborzi@gmail.com (M. Moradi)

http://www.acerp.ir/article_128022.html

Please cite this article as: Chameh, B., Moradi, M., Hajati, S., Alikhani Hessari, F., Kiani, M. A., "Synthesis and Characterization of Palladium Impregnated MIL-53(Fe) as Cathode Material of Supercapacitor", ***Advanced Ceramics Progress***, Vol. 7, No. 1, (2021), 11-16. https://doi.org/10.30501/acp.2020.250166.1045

scarcity and high cost [17-22]. The preparation of Pd@MOF-5 (1 wt. % Pd) was described by a solution of [Pd(acac)$_2$] in $CHCl_3$ and subsequent thermal hydrogenolysis of the intermediate material [Pd(acac)$_2$]x@MOF-5 (x 1⁄4 0.074). The authors did not provide information on the sizes of the Pd particles and distribution over the matrix [23]. In another study, Haruta et al. reported Au@MOFs (1–2 wt. percent au) and catalytic characteristics of liquid-phase aerobic alcohol oxidation [24].

In this research, the process of loading Pd nanoparticles on MIL-53(Fe) was carried out by facial hydrothermal method at room temperature. The electrochemical test of cyclic voltammetry on the fabricated electrode with synthesized materials was done the results of which showed improvement in the electrochemical performance of Pd/MIL-53(Fe), mainly due to an increase in the wettability and the specific surface area of MOF by Pd nanoparticles.

2. EXPERIMENTAL PROCEDURE

2.1. Materials

Iron chloride hexahydrate ($FeCl_3 \cdot 6H_2O$), N,N-dimethylformamide (DMF), terephthalic acid (1,4-BDC), hydrofluoric acid 48%, sodium tetrachloropalladate (II), 98% (Na_2PdCl_4), and sodium tetrahydridoborate, >98% ($NaBH_4$) were used without further purification. All chemicals used in this study were of commercially available analytical grade.

2.2. Synthesis of MIL-53(Fe)

MIL-53(Fe) was synthesized through the following procedure. First, $FeCl_3$. $6H_2O$ (10 mmol, 2.7 g), N,N-dimethylformamide (DMF) (50 mL), aqueous HF (10 mmol, 0.2 g), and 1,4-benzenedicarboxylic acid (H_2BDC) (10 mmol, 1.66 g) were mixed and stirred for 30 min; then, the mixture was placed in a Teflon-lined steel autoclave. The mixture was heated in a preheated fan oven at 150 ˚C for three days. Followed by cooling the autoclave to room temperature, MIL-53(Fe)[DMF] powder was recovered by filtration and washed with MeOH to obtain MIL-53(Fe)[MeOH]. MIL-53(Fe) was eventually achieved after MIL-53(Fe) [MeOH] had been washed with water and dried in air overnight [20].

2.3. Synthesis of Pd/MIL-53(Fe)

All the reagents were used without further purification. In this study, 10 mg of Na_2PdCl_4 was dissolved in 10 ml of deionized water to form a clear solution, which was subsequently poured into 10 mL of deionized water containing 200 mg of MIL-53(Fe). After thorough mixing, the resulting solution was stirred for 17 h at room temperature. Finally, 2.5 mg $NaBH_4$ dissolved in 5 ml deionized water was added to the previous mixture and stirred for 3 h. The as-obtained precipitates were then centrifuged and washed with ethanol and water for several times and dried at 70 °C for 24 h.

2.4. Materials characterization

X-Ray Diffraction (XRD, Philips X´pert diffractometer possessing Co Kα radiation, λ = 1.78 Å) was employed to explore the crystal phase of the materials at 40 kV and 30 mA with a 0.04 $^{\circ}s^{-1}$ step size. A pore size and surface area analyzer (Phschina, PHS 1020) were also used to extract the nitrogen adsorption/desorption isotherms at 77 K. Brunauer-Emmett-Teller (BET) theory was employed to determine the primarily specific surface area. The pore size and size distribution of the materials were calculated by the Barrett-Joyner-Halenda (BJH) method. Field Emission Scanning Electron Microscopy (FE-SEM, EDS, Tescan Mira3 Model) and Transmission Electron Microscopy (TEM, Philips EM208S) were employed to characterize materials morphology and chemical composition.

2.5. Electrochemical measurement

Electrochemical studies including Cyclic Voltammetry (CV) and Galvanostatic Charge-Discharge (GCD) were conducted at room temperature using an Origaflex Potentiostat/Galvanostat (OGF 500). The electrochemical measurements were conducted on a three-electrode system in 6 M KOH solution using a saturated calomel and Pt plate as reference and counter electrodes, respectively. In order to prepare working electrode, MIL-53(Fe) and Pd/MIL-53(Fe) were mixed with carbon black and Poly Vinylidine Difluoride (PVDF) at a mass ratio of 75:20:5 in NMP (N-Methyl-2-pyrrolidone) solution. Then, the mixture was homogenized by ultrasonication. After that, resultant slurry was sprayed on a nickel foam substratum with a mass load of ~1 mg/cm^2. The prepared electrodes were dried at 60 °C.

3. RESULTS AND DISCUSSION

The crystal structure of the as-prepared pure MIL-53(Fe) and Pd/MIL-53(Fe) composites is examined with X-ray diffraction (Fig. 1a). The characteristic peaks are at2θ = 10.53, 12.83, 14.61, 20.25, 21.41, 29.47, which confirm the well synthesis of MIL-53(Fe) due to being similar to those reported for standard MIL-53(Fe) [25]. The XRD pattern of Pd/MIL-53(Fe) shows that following the entrance of palladium to the system, the crystal structure of MIL-53(Fe) remains unchanged and peaks at 2θ of 14.61, 21.41, 29.47 decrease in intensity, thus attributing to loading of Pd nanoparticle on the MOF. N_2 adsorption–desorption isotherms of MIL-53(Fe) and Pd/MIL-53(Fe) (Fig. 1b) were employed to apply BET

theory for the determination of their specific surface area. MIL-53(Fe) and Pd/MIL-53(Fe) specific surface areas were found to be 12.8 and 16.4 m^2/g, respectively, showing an increase in the specific surface area of MIL-53(Fe) in the presence of palladium.

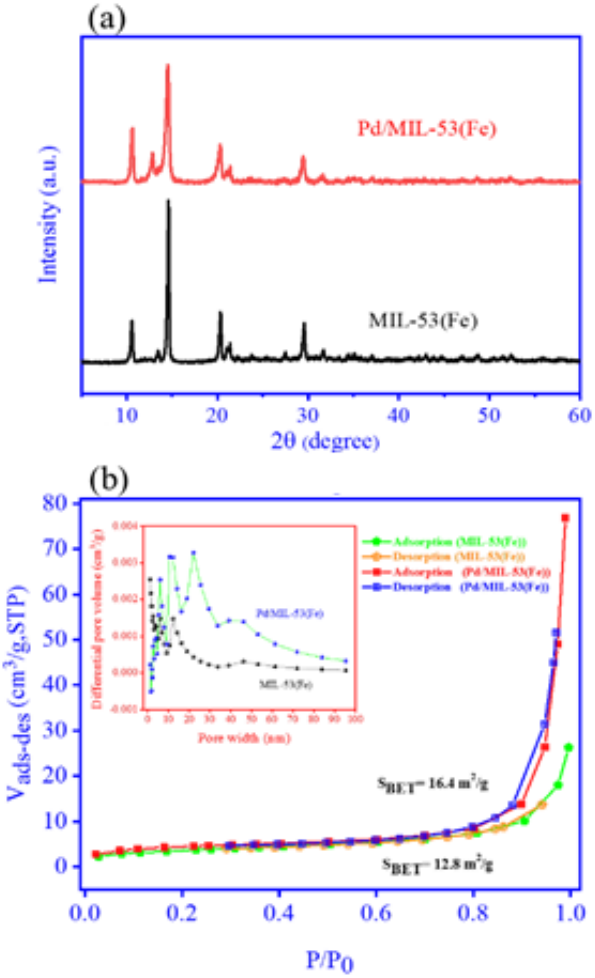

Figure 1. (a) XRD patterns of MIL-53(Fe) and Pd/MIL-53(Fe) and (b) BET isotherms and BJH (inset) of MIL-53(Fe) and Pd/MIL-53(Fe)

As seen in Fig. 1b, the adsorption and desorption branches of MIL-53(Fe) specify the presence of slit-like pores between sheets by sloping and covering a fairly wide range of P/P0 underlying the type-II isotherm with type-H3 hysteresis. The adsorption and desorption branches of Pd/MIL-53(Fe) are parallel and almost vertical corresponding to a hysteresis of type H1, which arises from a material with normal, even pores without interconnecting channels. These findings are in good agreement with the SEM image, demonstrating partly sheets and partly agglomerated particles. In Fig. 1b (inset), the BJH pore size distribution analysis reveals that these two samples have a generally meso-porous structure and only a limited number of pores with a size of less than 1 nm are present. Morphological analyses of as-synthesized materials are performed. Figs. 2a and 2b show SEM images of MIL-53(Fe) and Pd/MIL-53(Fe) composite.

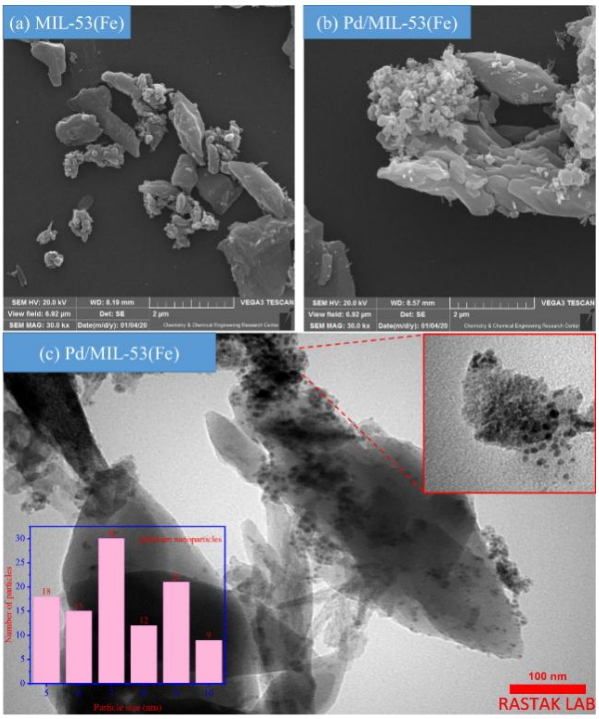

Figure 2. SEM image of (a) MIL-53(Fe), (b) Pd/MIL-53(Fe), and (c) TEM image of Pd/MIL-53(Fe)

As shown in Figs. 2a and 2b, the morphology of both samples is composed of partly sheets, agglomerated nanoparticle, and leaf-like structure with a dimension of 200 nm to 2 µm. For investigating the presence of palladium nanoparticles, the TEM analysis is employed in Figure 2c. According to the nanoparticles of Pd with a size under 20 nm, the MIL-53(Fe) was well decorated. The EDS spectrum of both samples is given in Figs. 3a and 3b.

Figure 3a confirms the XRD analysis and well synthesis of MOFs by elemental analysis. The presence of Cl beside other elements in Pd/MIL-53(Fe) in Fig. 3b might be attributed to the precursor of palladium. The atomic percentage of each element is given in Figures 3a and b. Another characterization was utilized to confirm the TEM image and presence of Pd in Pd/MIL-53(Fe). Atomic absorption spectroscopy confirms the 0.3 % of Pd in Pd/MIL-53(Fe).

The electrochemical performance of as-prepared MIL-53(Fe) and Pd/MIL-53(Fe) was employed to investigate the capacitive behavior of electrode materials with three-electrode cells using CV measurement in 6M KOH solution at room temperature. Fig. 4a and 4b represents the CV curves of MIL-53(Fe) and Pd/MIL-53(Fe) at different scan rates (in the range of 10–200 mV/s) in the −1 to 0 V potential window.

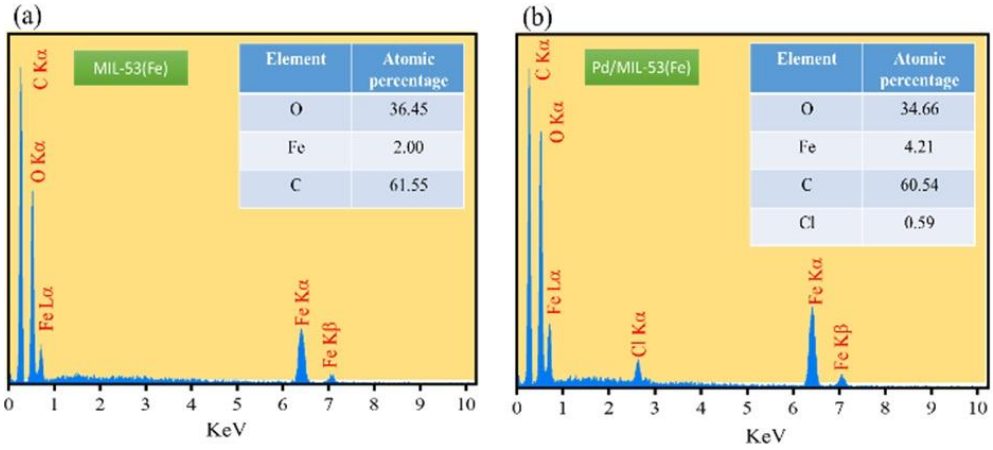

Figure 3. EDS spectrum of (a) MIL-53(Fe) and (b) Pd/MIL-53(Fe)

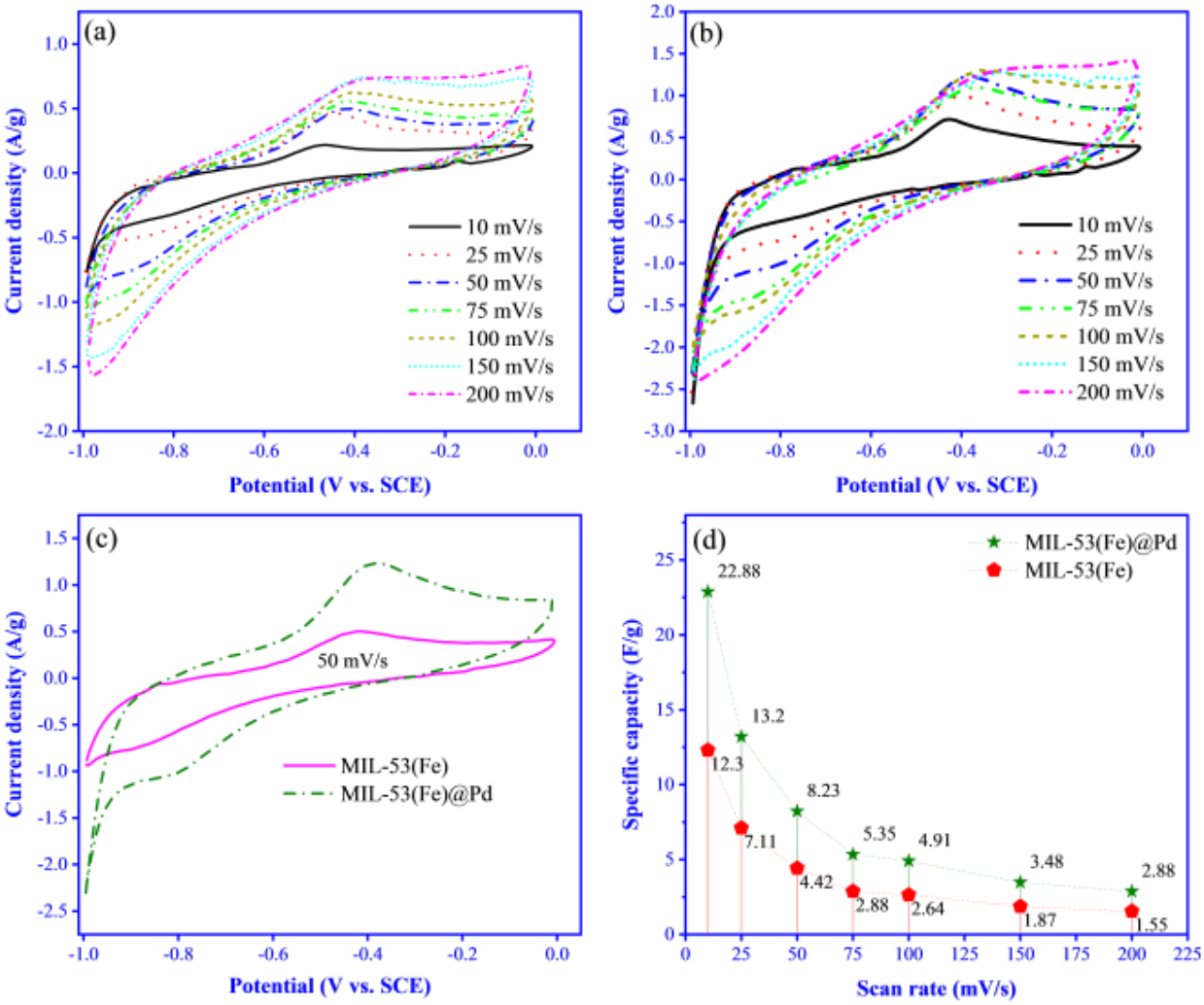

Figure 4. CV curve of (a) MIL-53(Fe) and (b) Pd/MIL-53(Fe) electrodes at different scan rate; (c) CV curve of MIL-53(Fe) and Pd/MIL-53(Fe) electrodes at a scan rate of 50 mV/s; (c) Specific capacitance of electrode materials at different scan rate from 10 to 200 mV/s

In the CV curves, both EDLC and Faradaic redox reactions control the capacitance characteristics. Contribution of EDLC can be inferred in the potential between -1 and -0.6 V from the curve of the CV with a partly rectangular structure. Furthermore, by increasing the scan rate, the cathodic peak shifted to negative potentials and the anodic peak shifted to positive potentials, which confirms that the redox processes take place easier in the nanocomposite samples. The characteristic of the reversible faradic conversion is Fe^{3+}/Fe^{2+} in MIL-53(Fe) and Pd/Pd^{2+} - Fe^{3+}/Fe^{2+} in Pd/MIL-53(Fe). Fig. 4c shows comparative CV curves for MIL-53(Fe) and Pd/MIL-53(Fe) composite electrodes at a scan rate of 50mV/s. CV curve of bare MIL-53(Fe) electrode is much narrower than the composite electrode. Higher capacitance of the composite electrode than MIL-53(Fe) electrode indicates the influence of palladium in composite with its redox reaction on electrochemical performance of MIL-53(Fe). Finally, the specific capacity of both samples according to Equation (1) was calculated and the plot of their specific capacity against scan rate is depicted in Figure 4d. The specific capacitance of the electrode was calculated from the CV curves according to following Equations [5]:

$$C_s = \int_{Va}^{Vc} \frac{IdV}{[(v \times (V_a - V_c) \times m)]} \quad (1)$$

where ∫ IdV denotes the integrated area under the CV plot loop, Cs represents the specific capacitance (F/g), υ corresponds to the scan rate (mV/s), (Va− Vc) shows the potential window (V), and m is the mass of active material. The Pd/MIL-53(Fe) has a specific capacity of 20.88 in 10 mV/s which is close to twice the value of MIL-53(Fe).

Galvanostatic Charge-Discharge (GCD) measurements were carried out at current densities of 0.5 A/g in order to assess the electrochemical performance and capacitance behavior of both electrodes. Figure 5a shows the comparison of GCD curves of MIL-53(Fe) and Pd/MIL-53(Fe) in the potential window between -1 and 0 V at current densities of 0.5 A/g. GCD curves possessed the platforms, showing that the capacitance is mostly governed by EDLC behavior of both samples by steep slope in the discharge section.

In addition, Pd/MIL-53(Fe) has a couple platform that can be related to the pseudocapacitive property that appears with the presence of palladium in composite as reflected in CV curves. The specific capacitance is also calculated through the following equation [5]:

$$C_s = \frac{I \times \Delta t}{m \times \Delta V} \quad (2)$$

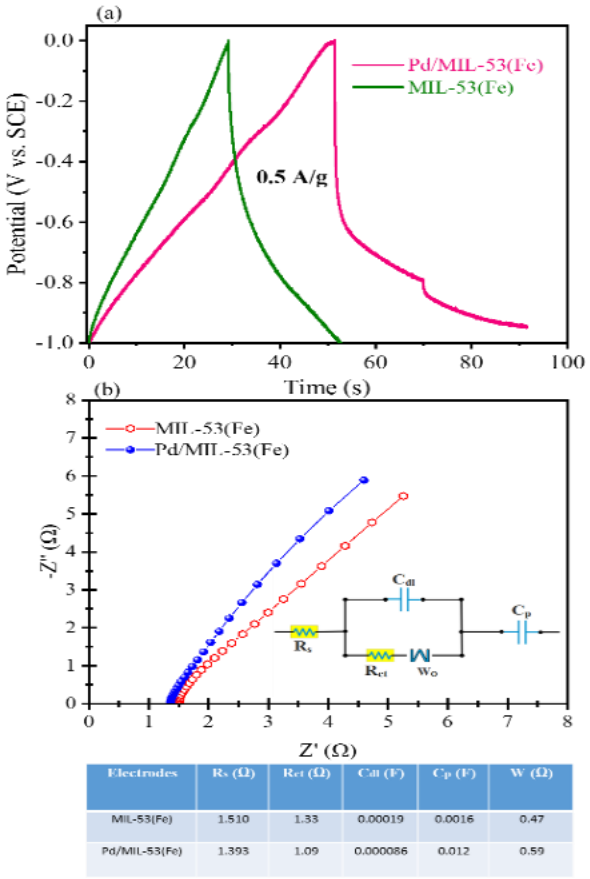

Electrodes	Rs (Ω)	Rct (Ω)	Cdl (F)	Cp (F)	W (Ω)
MIL-53(Fe)	1.510	1.33	0.00019	0.0016	0.47
Pd/MIL-53(Fe)	1.393	1.09	0.000086	0.012	0.59

Figure 5. (a) The comparison GCDs curves of MIL-53(Fe) and Pd/MIL-53(Fe) electrodes at current density of 0.5 A/g; (b) Impedance Nyquist plots at open circuit potential and the Electrical parameters of equivalent circuit

The specific capacity values of 10.1 and 19.9 F/g were achieved for MIL-53(Fe) and Pd/MIL-53(Fe), respectively. Also, the relation between capacitance of both electrodes and different current densities is reported in Fig. 6.

Electrochemical Impedance Spectroscopy (EIS) was employed to study the characteristic frequency response of MIL-53(Fe) and Pd/MIL-53(Fe) to investigate the interfacial kinetics of the electrochemical system. Figure 5b shows the Nyquist plots observed in the frequency range of 0.01 Hz to 100 kHz for samples with fitting circuit and widening semicircle area. The equivalent series resistance (Rs) values for MIL-53(Fe) and Pd/MIL-53(Fe) electrodes were determined at about 1.51 and 1.39 Ω. The diameter of the semicircle was related to the resistance of the charge transfer (Rct) and Pd/MIL-53(Fe) exhibited lower R_{ct} than MIL-53(Fe), which could be due to the good performance of its electron transport. Other values of the EIS fitting parameters are given in

Figure 5b. Pd/MIL-53(Fe) with a higher specific surface and higher conductivity of Pd nanoparticles improved the MOF efficiency by facilitating the diffusion of electrolytes and accelerating the transport of electrons.

The presence of palladium improved the electrochemical efficiency of bare MOFs by increasing the specific surface area and it yielded a larger number of active sites within the pores for quick electrochemical reactions. Also, it promoted the ions or electrons transfer at the electrolyte-electrode interface. Moreover, the presence of Pd in the redox reaction improved the capacitance behavior of the electrode.

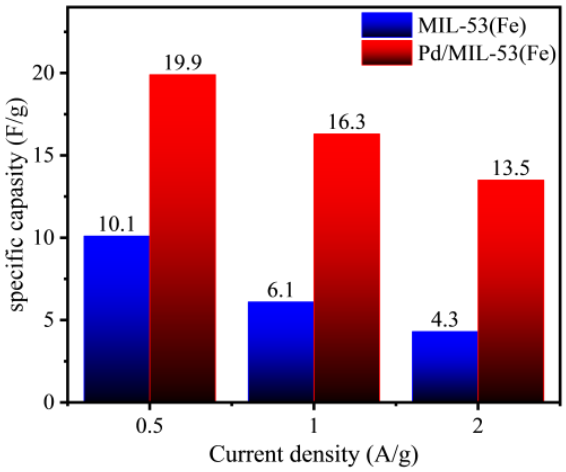

Figure 6. Relation of capacitance with current density

4. Conclusion

In summary, a simple strategy was used for the preparation and design of Pd/MIL-53(Fe) at room temperature. The TEM and Atomic absorption spectroscopy confirmed the loading of nanoparticle of Pd on the MOF. The electrochemical properties strongly depend on the CV cycles. The resulting Pd/MIL-53(Fe) demonstrated improved electrochemical efficiency compared to the bare MOF of MIL-53(Fe) by improving the specific surface area and further redox sites by joining palladium to redox reaction and doubling the specific capacity to 20.88 F/g. This work emphasizes the importance of optimizing the development and design of new materials such as MOFs.

ACKNOWLEDGEMENT

The present study was suported by Materials and Energy Research Center (MERC) through grant No 300647.

REFERENCES

1. Wang, Y. S., Chen, Y. C., Li, J. H., Kung, C. W., "Toward Metal–Organic-Framework-Based Supercapacitors: Room-Temperature Synthesis of Electrically Conducting MOF-Based Nanocomposites Decorated with Redox-Active Manganese", ***European Journal of Inorganic Chemistry***, Vol. 2019, No. 26, (2019), 3036-3044. https://doi.org/10.1002/ejic.201900676
2. Li, B., Wen, H. M., Cui, Y., Zhou, W., Qian, G., Chen, B., "Emerging multifunctional metal–organic framework materials ", ***Advanced Materials***, Vol. 28, No. 40, (2016), 8819-8860. https://doi.org/10.1002/adma.201601133
3. Lu, G., Li, S., Guo, Z., Farha, O. K., Hauser, B. G., Qi, X., Wang, Y., Wang, X., Han, S., Liu, X., DuChene, J. S., "Imparting functionality to a metal–organic framework material by controlled nanoparticle encapsulation", ***Nature Chemistry***, Vol. 4, No. 4, (2012), 310-316. https://doi.org/10.1038/nchem.1272
4. Chameh, B., Moradi, M., Hessari, F. A., "Decoration of metal organic frameworks with Fe_2O_3 for enhancing electrochemical performance of ZIF-(67 and 8) in energy storage application", ***Synthetic Metals***, Vol. 269, (2020), 116540. https://doi.org/10.1016/j.synthmet.2020.116540
5. Chameh, B., Moradi, M., Kaveian, S., "Synthesis of hybrid ZIF-derived binary ZnS/CoS composite as high areal-capacitance supercapacitor", ***Synthetic Metals***, Vol. 260, (2020), 116262. https://doi.org/10.1016/j.synthmet.2019.116262
6. Deng, T., Zhang, W., Arcelus, O., Wang, D., Shi, X., Zhang, X., Carrasco, J., Rojo, T., Zheng, W., "Vertically co-oriented two dimensional metal-organic frameworks for packaging enhanced supercapacitive", ***Communications Chemistry***, Vol. 1, No. 1, (2018), 1-9. https://doi.org/10.1038/s42004-017-0005-8
7. Farha, O. K., Eryazici, I., Jeong, N. C., Hauser, B. G., Wilmer, C. E., Sarjeant, A. A., Snurr, R. Q., Nguyen, S. T., Yazaydin, A. O., Hupp, J. T., "Metal–Organic Framework Materials with Ultrahigh Surface Areas: Is the Sky the Limit?", ***Journal of the American Chemical Society***, Vol. 134, No. 36, (2012), 15016-15021. https://doi.org/10.1021/ja3055639
8. Rodenas, T., Luz, I., Prieto, G., Seoane, B., Miro, H., Corma, A., Kapteijn, F., i Xamena, F. X. L., Gascon, J., "Metal–organic framework nanosheets in polymer composite materials for gas separation", ***Nature Materials***, Vol. 14, No. 1, (2015), 48-55. https://doi.org/10.1038/nmat4113
9. Corma, A., García, H., Llabrés i Xamena, F. X., "Engineering metal organic frameworks for heterogeneous catalysis", ***Chemical reviews***, Vol. 110, No. 8, (2010), 4606-4655. https://doi.org/10.1021/cr9003924
10. Horcajada, P., Chalati, T., Serre, C., Gillet, B., Sebrie, C., Baati, T., Eubank, J. F., Heurtaux, D., Clayette, P., Kreuz, C., Chang, J. S., "Porous metal–organic-framework nanoscale carriers as a potential platform for drug delivery and imaging", ***Nature Materials***, Vol. 9, No. 2, (2010), 172-178. https://doi.org/10.1038/nmat2608
11. Liu, Y. P., Zhao, S. F., Guo, S. X., Bond, A. M., Zhang, J., Zhu, G., Hill, C. L., Geletii, Y. V., "Electrooxidation of Ethanol and Methanol Using the Molecular Catalyst [{Ru4O4(OH)2(H2O)4}(γ-SiW10O36)2]10–", ***Journal of the American Chemical Society***, Vol. 138, No. 8, (2016), 2617-2628. https://doi.org/10.1021/jacs.5b11408
12. Deng, T., Lu, Y., Zhang, W., Sui, M., Shi, X., Wang, D., Zheng, W., "Inverted Design for High-Performance Supercapacitor Via $Co(OH)_2$-Derived Highly Oriented MOF Electrodes", ***Advanced Energy Materials***, Vol. 8, No. 7, (2018), 1702294. https://doi.org/10.1002/aenm.201702294
13. Chui, S. S. Y., Lo, S. M. F., Charmant, J. P., Orpen, A. G., Williams, I. D., "A Chemically Functionalizable Nanoporous Material $[Cu_3(TMA)_2(H_2O)_3]_n$", **Science**, Vol. 283, No. 5405, (1999), 1148-1150. https://doi.org/10.1126/science.283.5405.1148
14. Wang, L., Han, Y., Feng, X., Zhou, J., Qi, P., Wang, B.,"Metal–organic frameworks for energy storage: Batteries and

supercapacitors", ***Coordination Chemistry Reviews***, Vol 307, (2016), 361-381. https://doi.org/10.1016/j.ccr.2015.09.002
15. Hu, J., Wu, X., Zhang, Q., Gao, M., Qiu, H., Huang, K., Feng, S., Wang, T., Yang, Y., Liu, Z., Zhao, B., "Highly active PdNi/RGO/polyoxometalate nanocomposite electrocatalyst for alcohol oxidation", ***Langmuir***, Vol. 34, No. 8, (2018), 2685-2691. https://doi.org/10.1021/acs.langmuir.7b04031
16. Yan, Y., Wang, T., Li, X., Pang, H., Xue, H., "Noble metal-based materials in high-performance supercapacitors", ***Inorganic Chemistry Frontiers***, Vol. 4, No. 1, (2017), 33-51. https://doi.org/10.1039/c6qi00199h
17. Mensing, J. P., Lomas, T., Tuantranont, A.,"Ammonia strengthened graphene/CNT-wrapped polyaniline-nanofiber composites loaded with palladium nanoparticles for coin cell supercapacitors", ***Electrochimica Acta***, Vol. 263, (2018), 17-25. https://doi.org/10.1016/j.electacta.2017.12.193
18. Orooji, Y., Ghanbari, M., Amiri, O., Salavati-Niasari, M.,"Facile fabrication of silver iodide/graphitic carbon nitride nanocomposites by notable photo-catalytic performance through sunlight and antimicrobial activity", ***Journal of Hazardous Materials***, Vol. 389, (2020), 122079. https://doi.org/10.1016/j.jhazmat.2020.122079
19. Ghanbari, M., Salavati-Niasari, M.,"Tl_4CdI_6 nanostructures: facile sonochemical synthesis and photocatalytic activity for removal of organic dyes", ***Inorganic Chemistry***, Vol. 57, No. 18, (2018), 11443-11455. https://doi.org/10.1021/acs.inorgchem.8b01293
20. Karami, M., Ghanbari, M., Amiri, O., Salavati-Niasari, M., "Enhanced antibacterial activity and photocatalytic degradation of organic dyes under visible light using cesium lead iodide perovskite nanostructures prepared by hydrothermal method", ***Separation and Purification Technology***, Vol. 253, (2020), 117526. https://doi.org/10.1016/j.seppur.2020.117526
21. Gholamrezaei, S., Amiri, M., Amiri, O., Salavati-Niasari, M., Moayedi, H., "Ultrasound-accelerated synthesis of uniform $SrMnO_3$ nanoparticles as water-oxidizing catalysts for water splitting systems", ***Ultrasonics Sonochemistry***, Vol. 62, (2020), 104899. https://doi.org/10.1016/j.ultsonch.2019.104899
22. Tian, X. X., Gholamrezaei, S., Amiri, O., Ghanbari, M., Dashtbozorg, A., Salavati-Niasari, M., "Zn_2MnO_4/ZnO nanocomposites: One step sonochemical fabrication and demonstration as a novel catalyst in water splitting reaction", ***Ceramics International***, Vol. 46, No. 16, (2020), 25789-25801. https://doi.org/10.1016/j.ceramint.2020.07.058
23. Sabo, M., Henschel, A., Fröde, H., Klemm, E., Kaskel, S., "Solution infiltration of palladium into MOF-5: synthesis, physisorption and catalytic properties", ***Journal of Materials Chemistry***, Vol. 17, No. 36, (2007), 3827-3832. https://doi.org/10.1039/b706432b
24. Ishida, T., Nagaoka, M., Akita, T., Haruta, M., "Deposition of gold clusters on porous coordination polymers by solid grinding and their catalytic activity in aerobic oxidation of alcohols", ***Chemistry–A European Journal***, Vol. 14, No. 28, (2008), 8456-8460. https://doi.org/10.1002/chem.200800980
25. Zhang, Y., Li, G., Lu, H., Lv, Q., Sun, Z., "Synthesis, characterization and photocatalytic properties of MIL-53 (Fe)–graphene hybrid materials", ***RSC Advances***, Vol. 4, No. 15, (2014), 7594-7600. https://doi.org/10.1039/c3ra46706f